

Research Article

<https://doi.org/10.1631/jzus.A2500327>



Robust self-triggered switching control of autonomous ground vehicles with varying linear parameters

Yuanlong XIE¹, Shuting WANG¹, Liquan JIANG^{2,3,✉}, Hu LI¹, Hao WU¹, Sheng-quan XIE⁴

¹School of Mechanical Science and Engineering, Huazhong University of Science and Technology, Wuhan 430074, China

²State Key Laboratory of New Textile Materials and Advanced Processing Technologies, Wuhan Textile University, Wuhan 430200, China

³Hubei Key Laboratory of Digital Textile Equipment, Wuhan Textile University, Wuhan 430200, China

⁴School of Electronic and Electrical Engineering, University of Leeds, Leeds LS2 9JT, UK

Abstract: We propose a robust self-triggered switching control scheme for four-wheel-steering autonomous ground vehicles (FAGVs) to enhance tracking precision in the face of significant parameter variations. First, using the polytopic mechanism, the nonlinear dynamics of an FAGV are formulated as a switched linear parameter-varying system to accommodate parametric perturbations. With suitable dwell time, a novel self-triggered switching law is designed using energy density in terms of the tracking accuracy and system robustness; this satisfies the required control criteria while also preventing the Zeno phenomenon caused by traditional high-frequency switching. Through the application of multiple parameter-correlated Lyapunov functions, the resultant closed-loop system is ensured to be asymptotically stable with suitable auto-tuned gains. Finally, the efficacy and superiority of the proposed method are verified through experiments with an FAGV system.

Key words: Varying linear parameters; Autonomous ground vehicle; Switching controller; Zeno avoidance; Robust control


1 Introduction

Due to their high efficiency and operational consistency, intelligent vehicles have attracted substantial attention within the field of robotics and control (Jiang et al., 2022; Meng et al., 2023). Among existing platforms, four-wheel-steering autonomous ground vehicles (FAGVs) demonstrate superior omnidirectional maneuverability and motion capability compared with their differential-drive or mecanum-wheeled counterparts (Zhang JD et al., 2024; Arega et al., 2025). Equipped with independently actuated chassis and steering mechanisms, FAGVs can perform collision-avoiding maneuvers and achieve rapid trajectory tracking in constrained or complex environments (Vošahlík and Haniš, 2023; Menyechel Eneyew et al., 2025). In practical scenarios such as mobile machining, these vehicles are expected to follow prescribed trajectories across diverse

terrains, thereby imposing stringent requirements on controller performance (Lu et al., 2024; Yareshe et al., 2025). However, FAGVs often exhibit strong nonlinearities, significant disturbances, and tightly coupled position-attitude dynamics, all of which complicate the design of robust trajectory-tracking control for real-world deployment.

In recent years, extensive research has focused on control synthesis for mobile robots (Nguyen et al., 2024; Dirara et al., 2025). Kinematic model-based controllers have long been studied due to their simplicity and ease of implementation, exhibiting various attractive theoretical properties (Xie et al., 2022; Dersch et al., 2023; Metekia et al., 2025). However, such approaches neglect the effects of driving/braking forces and tire skidding, thereby limiting their effectiveness in practical applications. As an alternative, direct yaw moment control (DYMC) enhances stability and tracking performance by regulating longitudinal driving forces to generate corrective yaw moments (Zhang et al., 2023; Liang et al., 2024). The development of an effective DYMC strategy relies on an accurate dynamic model; however, such models typically contain uncertainties arising from unmodeled structural effects

✉ Liquan JIANG, lqjiang@wtu.edu.cn

 Liquan JIANG, <https://orcid.org/0000-0002-7203-5953>

Received July 23, 2025; Revision accepted Dec. 21, 2025;
Crosschecked Mar. 15, 2026; Online first Apr. 25, 2026

© Zhejiang University Press 2026

and external disturbances present in real environments (Ji et al., 2023). Additionally, key system parameters may undergo considerable variations under complex operating conditions, rendering constant-model-based control schemes unreliable, since fixed approximated models cannot capture the true dynamic response of an FAGV (Ma et al., 2023). This presents significant challenges to achieving robust tracking performance in harsh working conditions. Consequently, a DYMC method capable of accommodating parameter variations is essential for robust trajectory-tracking control of an FAGV.

Linear parameter-varying (LPV) control has shown promise in addressing perturbations caused by parameter variations of objectives (Abbas, 2024). Due to the difficulty of analytically identifying nonlinear terms, approximating complex system behavior as linear models parameterized with nonstationary parameters has emerged as a reasonable solution (Verhoek et al., 2024). This approximation works well because time-varying parameters reflect the system's operating points and an estimated LPV model can represent the actual system. Lyapunov functions provide useful options for designing controllers for LPV systems (Dehghani, 2024). However, a single LPV model may not be a sufficient approximation for highly demanding specifications or large-scale parameter variations. As such, a single Lyapunov function-based scheme may not meet the control requirements. Instead, multiple LPV controllers have been designed, which adopt different parameter subregions to gradually schedule the system model (Esmaeili and Modares, 2024). An appropriate control law can then be developed by using a detectable switching signal to specify the LPV systems (referred to as switched LPV systems) among several transition parameters, ensuring asymptotic stability and transient performance of the closed-loop system (Rotondo et al., 2022). This improves the dynamical approximation and control accuracy.

Switched LPV systems have been explored for four-wheeled mobile robots (Liu and Long, 2022). However, achieving a hybrid switching law has been challenging because the external switching signal is described in a sequence or fixed-time mechanism. This may lead to unnecessarily frequent switching, i.e., the Zeno phenomenon, and thus limit real-world implementation. Additionally, measurement noises and unreliable sensor transmission make it difficult to detect

the external switching signal for industrial FAGVs (Zhao et al., 2023). Therefore, a natural question arises: how can one design a switching control law for the derived LPV models that accurately represent an FAGV system? This paper aims to address this practical question.

Disturbances are ubiquitous in practical systems and may severely degrade control performance (Yang et al., 2024; Zeng et al., 2024). For switched LPV systems subjected to multiple disturbances, a common approach is to co-design a disturbance observer and a switching controller (Zhang S et al., 2024; Mohammed et al., 2025). However, the integrated structure of such methods often introduces switching bumps, which can produce undesirable transient behaviors or even destabilize the system in the case of large or lumped disturbances. Consequently, the stability guarantees provided by these approaches may be insufficient for industrial FAGV applications. Given that stability is a central requirement in control system design, it is vital to develop methods capable of attenuating multiple disturbances while ensuring enhanced robustness and switching performance for FAGVs.

To address the aforementioned issues, we propose an LPV switching system for FAGVs subjected to multiple disturbances. The main contributions of this study are as follows:

1. Compared with traditional kinematic or constant-parameter dynamic models (Peng et al., 2020; Guo et al., 2021), the LPV framework better captures the substantial parameter variations inherent in FAGV systems and better meets the practical operating requirements. This modeling approach enhances both accuracy and adaptability to industrial environments, thereby supporting real-time implementation and improving operational robustness.

2. Unlike existing sequential or time-driven switching laws prone to Zeno behavior (Cui et al., 2023; Zhao and Yang, 2024), the proposed approach employs an energy density, state-dependent, self-triggered mechanism that inherently reflects tracking accuracy and robustness. Without relying on external switching signals, it regulates tracking error through explicit performance measures and unifies the dwell-time constraint with the self-triggering rule through multiple Lyapunov functions.

3. The control gains of the switched system are scheduled online, thereby eliminating the need for

manual gain tuning. By simultaneously accounting for all potential operating conditions, the controller automatically adjusts its gains to accommodate the varying system dynamics. This ensures a desired level of disturbance attenuation across the entire operating range while enhancing the reliability and operational availability of the FAGV.

2 System modeling and problem formulation

2.1 Lateral motion modeling

As shown in Fig. 1, the trajectory tracking goal for the FAGV is to make the lateral offset (the distance from the center of gravity (CG) to the closest point on the reference path) and heading error (the error between the actual vehicle heading direction and the tangential direction of the desired path) zero, such that the system will track the desired path asymptotically. F_{xi} and F_{yi} represent the longitudinal and lateral tire forces of the i th tire, respectively, with $i=1, 2, 3, 4$ representing fl, fr, rl, and rr. The two-DOF (degree of freedom) dynamic model of FAGV is expressed as follows:

$$\begin{aligned}
 I_z \dot{\gamma} &= L_f(F_{yfl} + F_{yfr}) - L_r(F_{yrl} + F_{yrr}) + M_\omega, \\
 m v_x (\dot{\beta} + \gamma) &= F_{yfl} + F_{yfr} + F_{yrl} + F_{yrr}, \\
 M_\omega &= \sum_{i=1}^2 F_{xi} [(-1)^i L_f \cos \delta + L_f \sin \delta] + \sum_{i=3}^4 (-1)^i L_r F_{xi},
 \end{aligned} \tag{1}$$

where β and γ are the slip angle and yaw rate, respectively, m is the total mass, v_x is the longitudinal speed, I_z is the yaw inertia, δ is the steering angle of the front angle, L_f and L_r are the distances from the center of

gravity to the front and rear axles, respectively, and M_ω is the external yaw moment. The lateral forces related to the slip angle of the front and rear wheels are expressed as:

$$F_{yf} = K_f \alpha_f, \quad F_{yr} = K_r \alpha_r, \tag{2}$$

where F_{yf} and F_{yr} denote the generalized lateral tire forces of the front and rear tires, respectively (i.e., $F_{yf} = F_{yfl} + F_{yfr}$ and $F_{yr} = F_{yrl} + F_{yrr}$); K_f and K_r are the stiffness coefficients of the front and rear tires, respectively; α_f and α_r denote the slip angles of the front and rear wheels, respectively (as shown in Eq. (S1) of the electronic supplementary materials (ESM)).

In general, the tire cornering stiffness is influenced by load transfer. Under the small-angle approximations $\cos \delta \approx 1$ and $\sin \delta \approx 0$ (Ding et al., 2017), and combining Eqs. (1), (2), and (S1), we obtain a linearized model:

$$\begin{aligned}
 \dot{\beta} &= a_{11} \beta + a_{12} \gamma + b_{11} \delta, \\
 \dot{\gamma} &= a_{21} \beta + a_{22} \gamma + b_{21} \delta + b_{22} M_\omega,
 \end{aligned} \tag{3}$$

where the model parameters a_{11} , a_{12} , a_{21} , a_{22} , b_{11} , b_{21} , and b_{22} can be found in Eq. (S2) of the ESM.

By using $\mathbf{x} = [\beta, \gamma]^T$ and $\mathbf{u} = [\delta, M_\omega]^T$, we reformulate Eq. (3) into:

$$\dot{\mathbf{x}} = \mathbf{A}\mathbf{x} + \mathbf{B}\mathbf{u}, \tag{4}$$

with $\mathbf{A} = \begin{bmatrix} a_{11} & a_{12} \\ a_{21} & a_{22} \end{bmatrix}$ and $\mathbf{B} = \begin{bmatrix} b_{11} & 0 \\ b_{21} & b_{22} \end{bmatrix}$.

2.2 LPV modeling

Traditionally, to facilitate linearized modeling and subsequent practical implementation, many assumptions need to be made during the lateral modeling of FAGV shown in Eq. (1), such as constant speed and turning stiffness (Hu et al., 2016). However, in real-life situations, it is difficult to ensure accurate modeling with static parameters under time-varying working conditions and wheel stiffness. To capture time-varying perturbations and guarantee high modeling accuracy, we define an adjustment parameter vector $\boldsymbol{\rho}(t)$ to transfer the lateral control system Eq. (1) into a polytopic LPV system, which can be formulated as an affine function of the parameter vector $\boldsymbol{\rho}(t)$, i.e.,

$$\dot{\mathbf{x}}(t) = \mathbf{A}(\boldsymbol{\rho}(t))\mathbf{x}(t) + \mathbf{B}(\boldsymbol{\rho}(t))\mathbf{u} + \mathbf{C}(\boldsymbol{\rho}(t))\mathbf{w}(t), \tag{5}$$

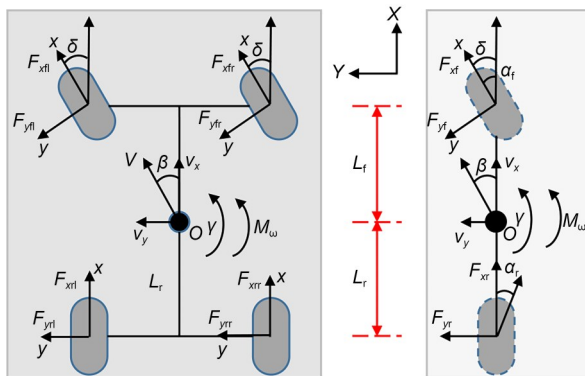


Fig. 1 FAGV coordinate system and forces: (a) four-wheel model; (b) single-track model

where $w(t)$ denotes the external disturbances, and $C(\rho(t))$ is the observation vector.

For convenience, $\rho(t)$ is simplified as ρ in the rest of this paper. With the vertex trajectory $\chi_1, \chi_2, \dots, \chi_N$, ρ can be represented by a polytopic LPV system, as derived in Eq. (S3) of the ESM, where $N=2^r$ (with r being the number of vertices), C_0 is the convex hull, and Φ denotes the parameter domain. For Eqs. (5) and (S3), the LPV system parameter matrix changes in the corresponding polytopic theories. Its vertices are composed of r local system matrices, as per Eq. (S4), where A_i and B_i denote the convex sets about χ_i in the range of Φ . During the construction of the abovementioned LPV system, $\varphi_i(t)$ denotes the time-varying weighting coefficient assigned to the i th local model, which is related to the scheduling parameters. For a scheduling parameter vector with r varying components, the corresponding LPV polytope consists of $N=2^r$ vertices, each representing an extreme combination of the parameter bounds. Through global linearization, the nonlinear FAGV dynamics subjected to disturbances can be approximated by an LPV representation. In this framework, a set of linear local models is obtained across the entire operating range, and the global LPV model is formed by selecting the appropriate local model associated with the current parameter vector $\varphi(t)$. This construction ensures that the state and scheduling parameters of the LPV system accurately capture the underlying FAGV dynamics.

2.3 Control objective

The control objective is to derive a robust self-triggered switching control solution that ensures the asymptotic stability of the polyhedral LPV system Eq. (5), in which the tracking error $e(t) = x_r(t) - x(t)$ satisfies the following performance indexes:

$$\int_0^t e^T(\tau) A e(\tau) d\tau \leq \lambda^2 \int_0^t \omega^T(\tau) \omega(\tau) d\tau, \quad (6)$$

where $\lambda > 0$ is the attenuation factor, A denotes a positive definite symmetric matrix, and x_r is the reference state. In this context, the stability of the resulting FAGV can be guaranteed under parameter perturbations such that the lateral offset and heading error can converge to zero.

For more details, the following lemmas are provided:

Lemma 1 (Souza et al., 2017) For a given matrix

$$M = \begin{bmatrix} m_{11} & m_{12} \\ * & m_{22} \end{bmatrix} < 0, \quad m_{11} = m_{11}^T \text{ and } m_{22} = m_{22}^T, \text{ one has } m_{11} < 0, m_{22} - m_{12}^T m_{11}^{-1} m_{12} < 0 \text{ and } m_{22} < 0, m_{11} - m_{12}^T m_{22}^{-1} m_{12} < 0.$$

Lemma 2 For real matrixes X and Y and a function matrix $Z(t)$ with suitable dimensions, if $Z(t)Z^T(t) \leq I$, we have $XZ(t)Y + Y^T Z^T(t)X^T \leq t^2 XX^T + t^{-2} Y^T Y, \forall t > 0$.

Lemma 3 For the known constant matrixes X and Y with appropriate dimensions and bounded function matrix $Z(t)$, if we have $Z(t)Z^T(t) \leq I$, when the symmetric matrix N satisfies $N + XZ(t)Y + Y^T Z^T(t)X^T < 0$, there exists a normal number t satisfying $A + t^2 XX^T + \frac{1}{t^2} Y^T Y < 0$.

3 Robust self-triggered control scheme

3.1 LPV switching controller design

We noted that using a single LPV model makes it difficult to satisfy the wide range of changing parameters caused by harsh working conditions and inherent perturbations. This inevitably leads to mismatches between the actual dynamics and the constructed control model. Given this context, the FAGV model can be established in a linear piecewise fashion to switch the parameters between several subregion sets. Each set is assigned to the related subsystem in an autonomous switching manner. The LPV model in Eq. (5) can be rewritten in a switched form with adjustable weighting parameters:

$$\dot{x}(t) = A_{\sigma_1(t)}(\varphi) x(t) + B_{\sigma_1(t)}(\varphi) u + C_{\sigma_1(t)}(\varphi) w(t), \quad (7)$$

where $\sigma_1(t): [0, \infty) \rightarrow H = \{1, 2, \dots, N\}$ denotes the switching signal used to characterize the activated models. For simplicity, we remove the symbol φ in the following discussion, so for instance, $A_{\sigma_1(t)}(\varphi)$ becomes $A_{\sigma_1(t)}$.

The reference model is considered as follows:

$$\dot{x}_r(t) = A_r x_r(t) + \Xi(t), \quad (8)$$

where A_r and $\Xi(t)$ denote the ideal parameter vector and input vector, respectively. We define an augmented system as described in Eq. (S5) of the ESM, with

$$\mathcal{X}(t) = [x(t) \quad x_r(t)]^T, \mathcal{A}_\sigma = \begin{bmatrix} A_{\sigma_1(t)} & 0 \\ 0 & A_r \end{bmatrix}, \mathcal{B}_\sigma = [B_{\sigma_1(t)} \quad 0]^T, \mathcal{C}_\sigma = [C_{\sigma_1(t)} \quad 0]^T, \text{ and } \tilde{\Xi}(t) = [0 \quad \Xi(t)]^T.$$

To ensure the control flexibility of the FAGV, a novel gain-scheduled switching controller is designed by:

$$\mathbf{u} = \mathbf{K}_\sigma(\mathbf{x}_r(t) - \mathbf{x}(t)) = \mathbf{K}_\sigma \mathbf{e}(t), \quad (9)$$

with $\mathbf{K}_\sigma = [k_1, k_2]$ being the control gain to be designed later (see Theorem 2 for more details). Note that the controller from Eq. (9) may be sensitive to small disturbances and uncertainties in implementation. Thus, we modify Eq. (9) to:

$$\mathbf{u} = \sum_{i=1}^{\eta} \sum_{j=1}^r \sigma_i \varphi_j(t) (\mathbf{K}_\sigma + \Delta \mathbf{K}_\sigma) \mathbf{e}(t), \quad (10)$$

where η is the switching subregion number, and $\Delta \mathbf{K}_\sigma$ is the gain increment satisfying:

$$\Delta \mathbf{K}_\sigma = \mathbf{R}_\sigma \mathbf{L}_\sigma(t) \mathbf{T}_\sigma, \quad (11)$$

with \mathbf{R}_σ and \mathbf{T}_σ being known matrices, and $\mathbf{L}_\sigma(t)$ meeting the requirement $\mathbf{L}_\sigma^T(t) \mathbf{L}_\sigma(t) \leq \mathbf{I}$. We derive the switching controller as:

$$\begin{aligned} \mathbf{u} &= \sum_{i=1}^{\eta} \sum_{j=1}^r \sigma_i \varphi_j(t) (\tilde{\mathbf{K}}_\sigma + \Delta \tilde{\mathbf{K}}_\sigma) \boldsymbol{\chi}(t), \\ \tilde{\mathbf{K}}_\sigma &= [\mathbf{K}_\sigma - \mathbf{K}_\sigma]^T, \quad \Delta \tilde{\mathbf{K}}_\sigma = [\Delta \mathbf{K}_\sigma - \Delta \mathbf{K}_\sigma]^T, \end{aligned} \quad (12)$$

where $\tilde{\mathbf{K}}_\sigma$ and $\Delta \tilde{\mathbf{K}}_\sigma$ are intermediate variables, and $\boldsymbol{\chi}$ is an augmented matrix of state variables.

Integration of Eqs. (S5) and (12) results in:

$$\dot{\mathbf{x}}(t) = \tilde{\mathcal{A}}_\sigma \boldsymbol{\chi}(t) + \tilde{\mathbf{E}}(t) + \mathcal{C}_\sigma \mathbf{w}(t), \quad (13)$$

where $\tilde{\mathcal{A}}_\sigma = \mathcal{A}_\sigma + \mathcal{B}_\sigma (\tilde{\mathbf{K}}_\sigma + \Delta \tilde{\mathbf{K}}_\sigma)$.

Remark 1 Compared with the nominal state-feedback law in Eq. (9), the modified controller in Eq. (10) introduces a structured and bounded gain perturbation, thereby improving robustness to disturbances and modeling uncertainties. In addition, the convex combination in Eq. (10) enables smooth gain scheduling across parameter regions, reducing high-frequency gain variations and limiting the amplification of measurement noise.

3.2 Robust self-triggered switching mechanism

Suppose there exists a family of positive definite matrix functions $\mathbf{Q}_k(t)$, and each of them is smooth over the corresponding parameter subset. The switching

signal σ determines the active operational region of the switched system and, consequently, the corresponding positive-definite matrix function. Based on this, we define multiple parameter-dependent Lyapunov functions, as shown in Eq. (S6) of the ESM.

In general, the stability of a switched LPV system does not necessarily depend on the constructed Lyapunov function V_σ strictly decreasing along the parameter trajectory. Instead, it is often sufficient to ensure that V_σ decreases within the active parameter region when designing a self-triggered switching rule that considers system mismatch oscillation and selects the optimal subsystem and corresponding controller. This approach limits the number of switches allowed over a finite time interval, thereby relaxing the continuous requirements under which the self-triggered switching rule is applied. Along this line, this relaxed stability condition provides enhanced control flexibility. In the following section, we will derive the synthesis conditions for the proposed switching LPV controller.

In switched LPV systems, frequent switching can cause oscillation and lead to the occurrence of the Zeno phenomenon. To address this issue, we make use of Lyapunov functions across the switching surfaces. A time interval t_T between two adjacent switching instants is specified in Eq. (S7) of the ESM, where $\kappa_1, \kappa_2, \dots, \kappa_r$ denote the switching instants.

We define $\kappa_{\tau, T_i} = \kappa_\tau + T_i$, $T_i = t_{T_1} + t_{T_2} + \dots + t_{T_i}$, $i \in N^+$, and t_{T_i} as the switching interval in the aperiodic cycle. Then, with $T_0 = 0$ and $\kappa_{\tau, T_0} = \kappa_\tau$, this implies that there is no switching within the time interval t_T . Furthermore, one can obtain that $\kappa_\tau + t_T \leq \kappa_{\tau+1, T_0} = \kappa_{\tau+1}$. In this study, the switching law related to parameter driving and dwell time are defined as:

$$\sigma(t) = \begin{cases} k, & t \in [\kappa_\tau, \kappa_\tau + t_T) \cup (\mathcal{X}, \varphi) \in Y_k, \\ j, & t \geq \kappa_\tau + t_T \text{ and } (\mathcal{X}, \varphi) \notin Y_k, \end{cases} \quad (14)$$

where $\sigma(t)$ represents the active LPV subsystem index, k is the current activated subsystem, Y_k denotes the parameter domain of k , and the switch time interval $[\kappa_\tau, \kappa_{\tau+1})$ is given in Eq. (S8) of the ESM.

Next, we define the function $V(\mathbf{Q}_k) = \boldsymbol{\chi}^T \mathbf{Q}_k \boldsymbol{\chi}$, and Y_k and Y_j are derived in Eq. (S9) of the ESM. For the switched LPV system, when the system satisfies Y_j , the switching is triggered autonomously, and the j th subsystem is activated. \mathbf{Q} is the positive defined matrix

with the appropriate dimensions. When $t \in [\kappa_\tau, \kappa_{\tau+1})$, the next switching time $t = \kappa_{\tau+1}$ is determined by Eq. (S10) of the ESM.

Referring to current research (Cui et al., 2023; Zhao and Yang, 2024), time-related switching among several subsystems is triggered periodically by receiving a switching signal online. However, in practical implementation, real-time monitoring may not be guaranteed, leading to time series inconsistencies due to factors such as the thread scheduling, resource allocation, computation time, and external environment. To overcome these limitations, we propose designing the switching signal using Eq. (S9) to achieve self-triggered switching and avoid the Zeno phenomenon caused by frequent switching. By expanding the switching condition Eq. (S8), we can redesign Y_j as shown in Eq. (S11) of the ESM.

Through the proposed method, the switching becomes nonperiodic in a self-triggered manner, thus reducing the controller's updating burden. Therefore, from the perspective of system switching conditions and self-triggered rules, the proposed scheme helps to improve the solvability of system switching.

Compared with the approaches in Qu et al. (2020) and Wang and Zhao (2017), we employ a parameter-dependent, time-varying positive-definite matrix function, enabling multiple Lyapunov functions to bound the tracking error within a small neighborhood. Moreover, by lowering the energy density at switching instants, the proposed method improves the overall stability of the system. Here, energy density is defined as a Lyapunov-based performance measure that reflects instantaneous tracking accuracy and robustness, serving as the triggering criterion for autonomous switching. In contrast to Wang and Zhao (2017), the proposed switched LPV framework enforces a dwell time greater than t_τ , thereby preventing Zeno behavior and reducing sampling-frequency requirements. Under this switching law, subsystem transitions occur only when condition Eq. (S10) is satisfied, yielding a robust self-triggered switching control strategy for mobile robots. This is established explicitly in the following theorem.

Theorem 1 For a switching LPV system subjected to disturbances, we define the positive numbers $\varphi_1, \varphi_2, \phi_1, \phi_2$, nonnegative weight function $\omega_{k,p}$, matrix function $\mathbf{K}_k, \Delta \mathbf{K}_k$, and positive definite matrices $\mathbf{Q}_{k,T_\tau}, \mathbf{Q}_{k,t}, \mathbf{P}_{k,T_\tau}, \mathbf{P}_{k,t}, \mathbf{Q}_{j,T_0}, \mathbf{Q}_{j,T_1}$ for $k, j \in H, j \neq k$, provided the following inequalities hold:

$$\begin{bmatrix} \mathcal{P}_{11} & \mathcal{P}_{12} \\ \mathcal{P}_{21} & \mathcal{P}_{22} \end{bmatrix} < 0, \quad \begin{bmatrix} \mathcal{R}_{11} & \mathcal{R}_{12} \\ \mathcal{R}_{21} & \mathcal{R}_{22} \end{bmatrix} < 0, \quad (15)$$

where detailed parameters are provided in Eq. (S12) of the ESM. Then, the constructed switching polyhedral LPV system is guaranteed to be asymptotically stable. The complete proof is provided in Section S2 of the ESM.

Remark 2 In practice, the dwell time t_τ is selected according to the physical limitations of the FAGV platform, such as the minimum time required for the system to exhibit a meaningful change in its Lyapunov energy. A larger dwell time prevents excessive switching and avoids actuator chattering, while a smaller value promotes responsiveness.

3.3 Gain-scheduling rule

To implement the proposed self-triggered controller, we need to jointly derive a set of state-feedback gains $\{K_1, K_2, \dots, K_N\}$ and the switching function to achieve an optimal solution. Remarkably, as demonstrated by the following results, the proposed gain-updating rule is not dependent on the system parameters, thus eliminating the need for online measurement.

Theorem 2 For an LPV system subjected to external disturbances, suppose there exist positive constants ϖ_1, ϖ_2 , matrices $\mathbf{Y}_{1k,l}, \mathbf{Y}_{2,l}, \mathbf{Y}_{1k,L}, \mathbf{Y}_{2,L}$, and positive definite matrices $\mathbf{Q}_{k,T_\tau}, \mathbf{Q}_{k,t}, \mathbf{P}_{k,T_\tau}, \mathbf{P}_{k,t}, \mathbf{Q}_{j,T_0}, \mathbf{Q}_{j,T_1}$ for $k, j \in H, j \neq k, l = 0, 1, \dots, L-1$. Then, the following holds:

$$\begin{bmatrix} \mathbf{A}_{j1} & \mathbf{A}_{j2} \\ * & \mathfrak{F} \end{bmatrix} < 0, \quad \begin{bmatrix} \mathbf{A}_{T1} & \mathbf{A}_{T2} \\ * & \mathfrak{F} \end{bmatrix} < 0, \quad (16)$$

where detailed parameters are provided in Eq. (S13) of the ESM. Consequently, the designed controller guarantees disturbance suppression, and the controller gain is determined by:

$$\hat{\mathbf{K}}_k = \begin{cases} \frac{[\mathbf{Q}_{k,T_i} + l(\mathbf{Q}_{k,T_{i+1}} - \mathbf{Q}_{k,T_i})]}{[\mathbf{P}_{k,T_i} + l(\mathbf{P}_{k,T_{i+1}} - \mathbf{P}_{k,T_i})]}, & t \in [\kappa_{\tau,T_i}, \kappa_{\tau,T_{i+1}}), \\ \mathbf{Q}_{k,t}, \mathbf{P}_{k,t}^{-1} & t \in [\kappa_\tau, \kappa_{\tau,T_1}) \cup [\kappa_{\tau,T_i}, \kappa_{\tau+1}). \end{cases} \quad (17)$$

The complete proof is provided in Section S3 of the ESM.

Remark 3 For the active subsystem k and the current time interval $[\kappa_{\tau,T_i}, \kappa_{\tau,T_{i+1}})$, the matrices $\mathbf{Q}_k(t)$ and $\mathbf{P}_k(t)$

are obtained by linear interpolation, and the scheduled gain is computed explicitly according to Eq. (17). Since the system order is low, this matrix inversion can be performed in real time with negligible computational cost; as a result, the proposed gain-scheduling strategy is practically feasible for industrial FAGV platforms.

Remark 4 Although Theorems 1 and 2 involve multiple matrix inequalities, all decision variables are linear, representing a convex semidefinite programming problem. Therefore, the controller gains and Lyapunov matrices can be obtained online using standard linear matrix inequality (LMI) solvers (e.g., the MATLAB LMI Toolbox), ensuring that the method is practical and computationally lightweight.

By using the abovementioned solution, the LPV switching controller can be treated as a single entity, with the gain scheduling achieved entirely by the state-dependent controller. This allows for a more streamlined and efficient approach to control design, with improved stability and reduced sampling-frequency requirements.

4 Experiments and results

4.1 Experimental setup

To verify the feasibility of the proposed control strategy, we conducted experimental verification on an FAGV in a laboratory setting (shown in Fig. 2). The platform is equipped with an industrial personal computer (PC), light detection and ranging (LiDAR), and an industrial camera and is highly adaptable and flexible due to its independent drive and steering actuation features. During automatic operation, sensor data

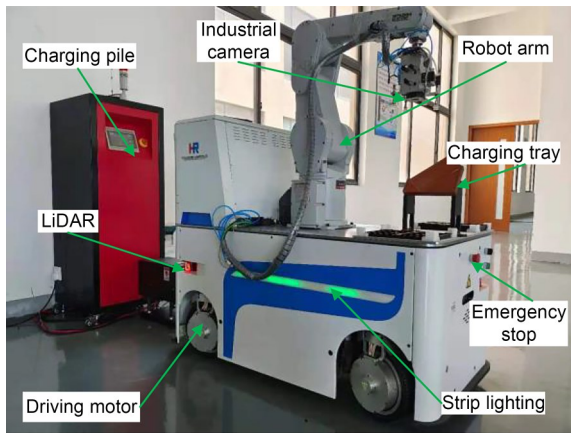


Fig. 2 Developed FAGV

from the LiDAR, inertial measurement unit (IMU), accelerometer, and encoder are fused to obtain real-time information on the yaw rate and sideslip angle, enabling DYMC lateral stabilization control.

In this paper, the relevant control parameters are specified as follows: $t_r=1$ s, $\omega_1=\omega_2=1$, $\phi_1=\phi_2=\phi_1=\phi_2=1$, $m=700$ kg, $L_f=L_r=0.48$ m, and $I_z=130$ kg·m². To demonstrate the effectiveness of the proposed method, we compared it with several other control schemes suitable for FAGVs, including: (1) a conventional proportion integration differentiation (PID) control scheme, where the parameters were manually tuned ($k_p=1.2$, $k_i=k_d=0.6$); (2) a sliding mode control (SMC) method; (3) the proposed LPV method with fixed gains (referred to as F-LPV). In the experiment, a sampling time of 1 ms was used. The scheduling parameter is the steering angle, and its range of values is $\phi \in (0, 0.35)$ rad. The scheduling parameter range can be divided into two subsets, and the DYMC control of the mobile robot can be described as a switched LPV model with two subsystems using the two different subsets with scheduling factors. In practical implementation, the matrix parameters of this model can be expressed as:

$$\begin{aligned}
 A_1 &= \begin{bmatrix} 61.9048 & -13.3810 \\ -7.3846 & -38.4129 \end{bmatrix} + \\
 &\quad \phi \begin{bmatrix} 0.6918 & 0.2767 \\ 2.1456 & -0.8582 \end{bmatrix}, \\
 A_2 &= \begin{bmatrix} 41.9048 & -7.7048 \\ -1.8462 & -25.9838 \end{bmatrix} + \\
 &\quad \phi \begin{bmatrix} 0.4683 & 0.1499 \\ 1.8155 & -0.5810 \end{bmatrix}, \\
 B_1 &= \begin{bmatrix} 15.4762 & 0 \\ 8.9143 & 1 \end{bmatrix} + \phi \begin{bmatrix} -0.6918 & 0 \\ -2.1456 & -0.0215 \end{bmatrix}, \\
 B_2 &= \begin{bmatrix} 10.5714 & 0 \\ 7.5429 & 1 \end{bmatrix} + \phi \begin{bmatrix} -0.6386 & 0 \\ -1.8155 & -0.0472 \end{bmatrix}.
 \end{aligned}$$

4.2 Results and discussion

The following two cases with different reference profiles are conducted to validate the proposed method.

In Case 1, the proposed method is compared with the PID, SMC, and F-LPV controllers in terms of yaw-rate and sideslip-angle tracking performance. As shown in Figs. 3 and 4, all methods exhibit stable lateral tracking. To further verify the superiority of the proposed method, the maximum error (MAX), mean absolute error (MAE), and root-mean-squared error (RMSE) of each controller are reported in Table 1. For instance,

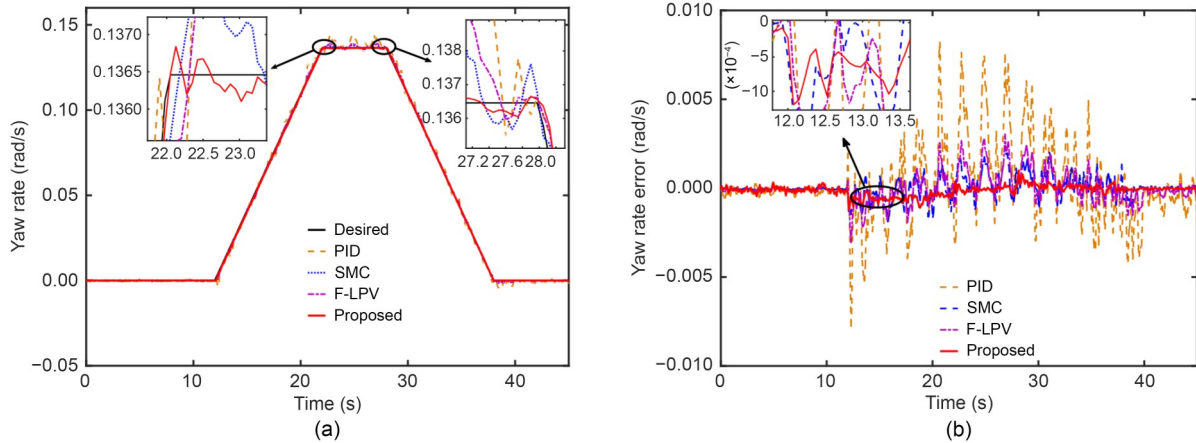


Fig. 3 Yaw rate tracking performance in Case 1: (a) tracking response; (b) tracking error

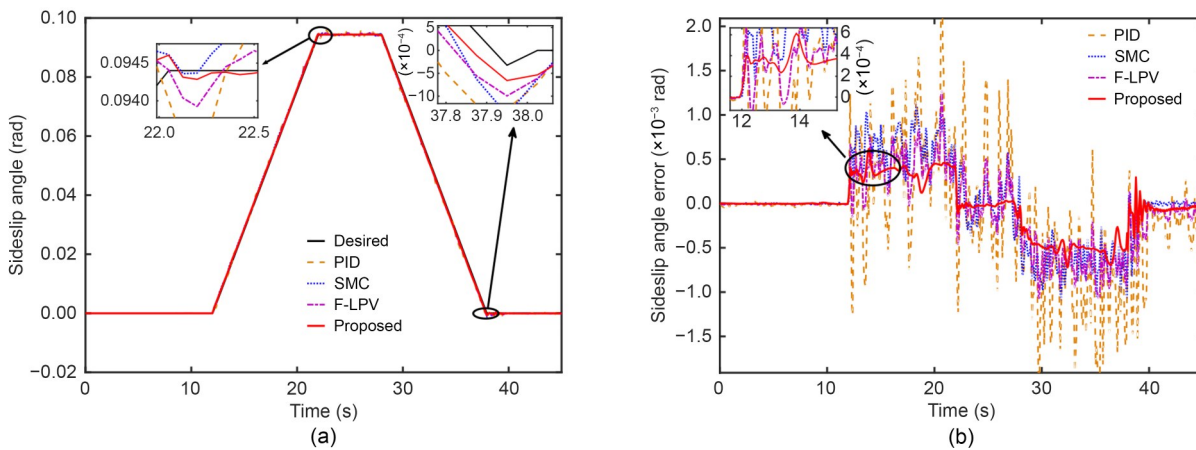


Fig. 4 Sideslip angle tracking performance in Case 1: (a) tracking response; (b) tracking error

Table 1 Criteria under comparison controllers in Case 1

State	Method	Criteria ($\times 10^{-4}$)		
		MAX	MAE	RMSE
Yaw rate (rad/s)	PID	82.41	28.32	13.01
	SMC	34.64	13.61	5.74
	F-LPV	32.17	14.39	6.32
	Proposed	13.33	4.86	2.98
Sideslip angle (rad)	PID	27.03	8.37	5.53
	SMC	12.15	3.26	1.37
	F-LPV	13.57	3.81	1.82
	Proposed	6.85	0.94	0.32

the yaw-rate overshoot values of the PID, SMC, and F-LPV methods are 0.0082, 0.0034, and 0.0032 rad/s, respectively, whereas the proposed method limits the overshoot to 0.0013 rad/s. This corresponds to reductions of 84.15%, 61.76%, and 59.38%, demonstrating that the proposed controller effectively suppresses

overshoot and enhances the overall tracking performance. Moreover, excellent sideslip-angle responses can be observed in Fig. 4, and the error metrics in Table 1 further confirm the improved tracking accuracy of the proposed method. The corresponding control signals, including the yaw moment, steering angle, switching signal, and time-varying control gain, are presented in Figs. 5 and 6. As illustrated in Fig. 6, the control gain is updated in real time based on environmental variations using the multi-parameter Lyapunov framework. Meanwhile, the switching signal assists the controller in selecting the most appropriate subsystem parameters, thereby ensuring satisfactory tracking performance. In addition, Table 2 provides the timing characteristics of the controllers. Although the proposed method has a somewhat longer computation period due to the matrix operations required by the LMI-based gain scheduling module, the switching mechanism enables the controller to select parameters better suited to the current

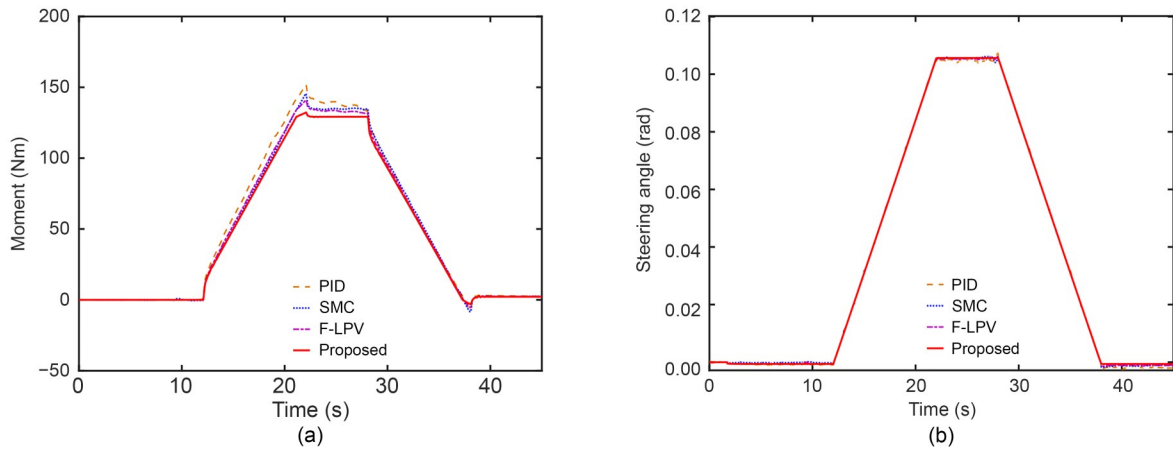


Fig. 5 Control inputs in Case 1: (a) moment input; (b) steering angle input

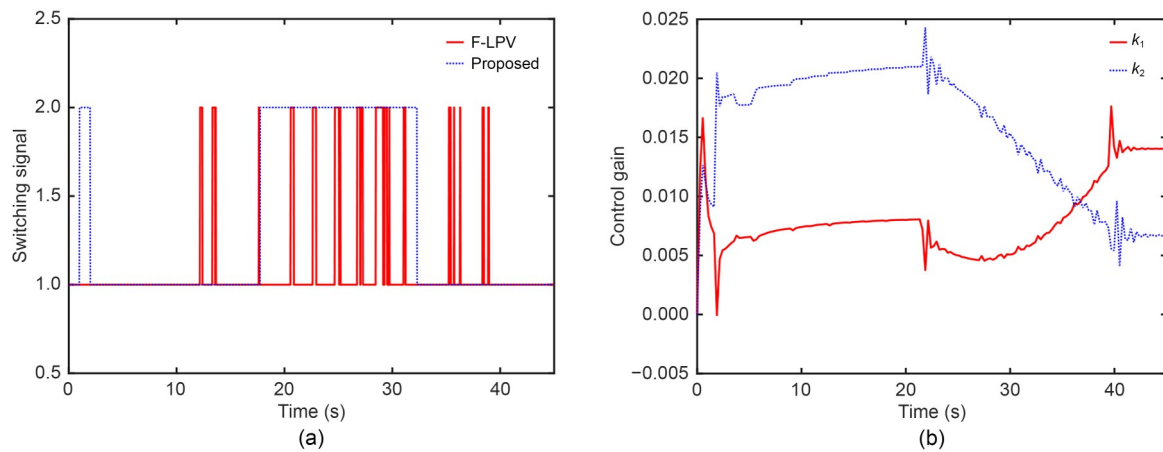


Fig. 6 Switching signal and control gain in Case 1: (a) switching signal; (b) control gain

Table 2 Consumed time of the comparison methods in Case 1

Method	Consumed time (ms)		
	MAX	MAE	RMSE
PID	21.0721	11.1961	2.8159
SMC	23.3469	12.1070	2.9014
F-LPV	30.9445	14.1379	3.3162
Proposed	32.6101	15.5374	3.4576

operating conditions; the ultimate result is more rapid error convergence. Consequently, the proposed method achieves superior control performance overall.

In Case 2, Fig. 7 illustrates the yaw-rate tracking responses and corresponding error curves, and all compared methods achieve closed-loop tracking of the reference trajectory. However, the PID, SMC, and F-LPV controllers exhibit pronounced oscillations during tracking, whereas the proposed method reaches a stable state more rapidly, particularly during turning maneuvers. The error curves in Fig. 7 further show that the PID,

SMC, and F-LPV methods produce overshoot values of 0.0174, 0.0122, and 0.0089 rad/s, respectively, while the proposed method limits the overshoot to 0.0061 rad/s. By suppressing undesirable overshoot, the proposed method significantly enhances tracking accuracy and smoothness, thereby outperforming the benchmark controllers. A similar conclusion can be drawn from the sideslip-angle tracking responses and error curves in Fig. 8. The PID controller exhibits large oscillations and pronounced peaks during state transitions, while the proposed method demonstrates greater robustness and accuracy than the SMC and F-LPV approaches. The variation of the control input signals is shown in Fig. 9. The switching signal and scheduled control gain are shown in Fig. 10. Our approach employs a real-time switching mechanism that selects the most suitable subsystem model based on environmental variations and the multi-parameter Lyapunov function. This enables the controller to effectively adapt to changing operating

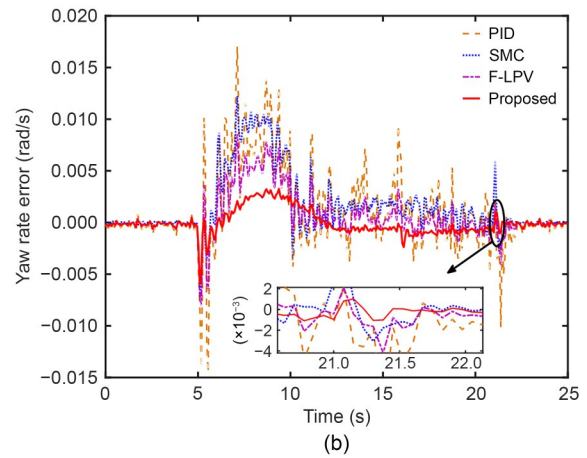
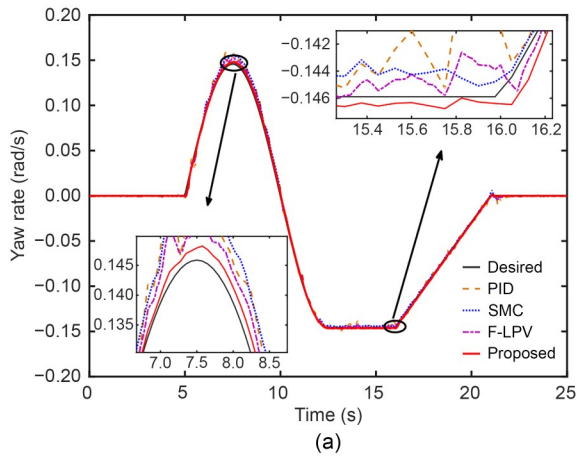


Fig. 7 Yaw rate tracking performance in Case 2: (a) tracking response; (b) tracking error

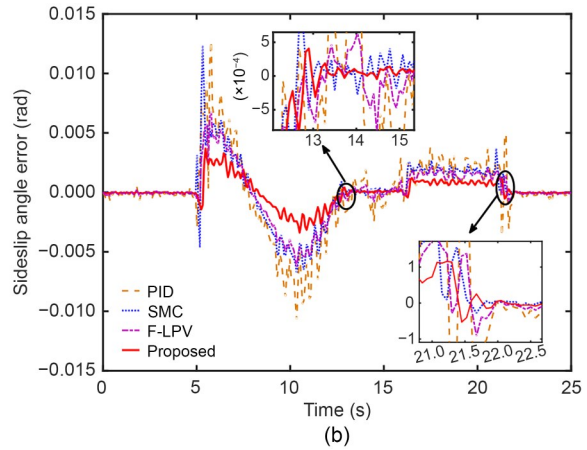
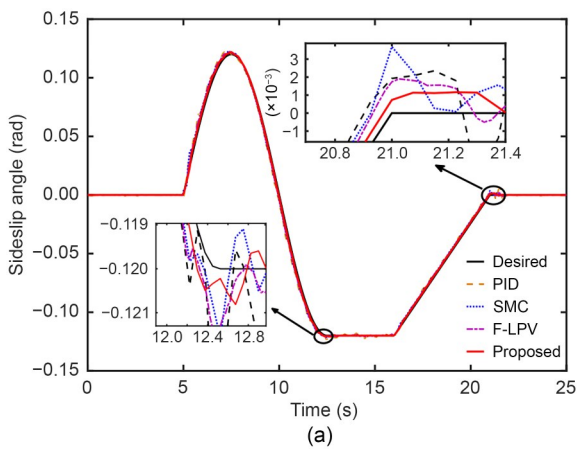


Fig. 8 Sideslip angle tracking performance in Case 2: (a) tracking response; (b) tracking error

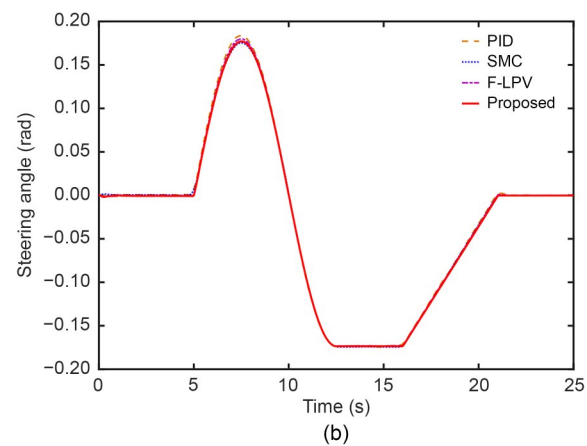
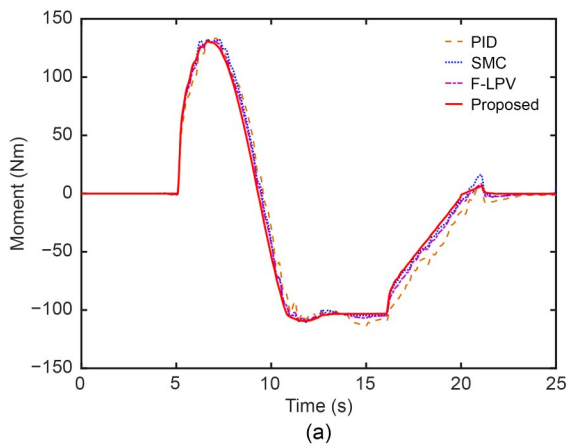


Fig. 9 Control inputs in Case 2: (a) moment input; (b) steering angle input

conditions, thereby enhancing the robustness and tracking performance. The corresponding error metrics for this scenario are summarized in Table 3. Additionally, as depicted in Fig. 10, the adaptively scheduled

control gains further improve the controller's ability to respond to variations in the external environment and operating conditions, leading to enhanced tracking accuracy.

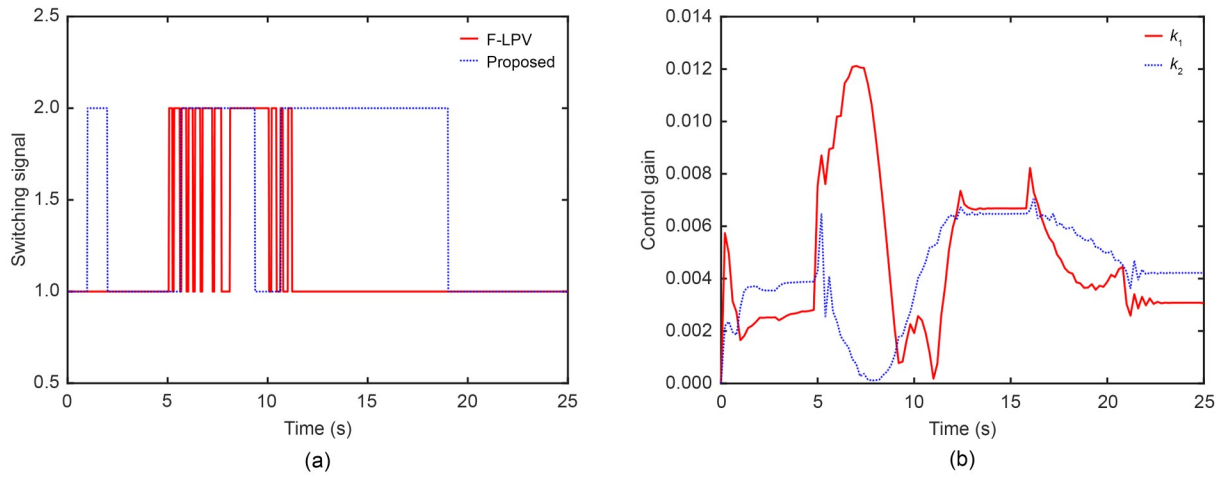


Fig. 10 Switching signal and control gain in Case 2: (a) switching signal; (b) control gain

Table 3 Criteria under comparison controllers in Case 2

State	Method	Criteria ($\times 10^{-4}$)		
		MAX	MAE	RMSE
Yaw rate (rad/s)	PID	174.07	32.16	27.84
	SMC	122.39	25.42	21.46
	F-LPV	89.57	19.80	18.54
	Proposed	61.77	9.68	8.27
Sideslip angle (rad)	PID	138.51	21.11	17.57
	SMC	133.12	14.29	9.64
	F-LPV	68.75	12.60	7.37
	Proposed	37.48	3.27	1.04

Overall, our method provides a smoother and more stable tracking effect for the FAGV, demonstrating its superiority to traditional control methods. These results suggest that the proposed method has significant potential for practical applications.

5 Conclusions

To address the challenges posed by time-varying parameters in FAGVs under lateral dynamic control, we established a robust self-triggered switching tracking control method that utilizes a multi-parameter correlation Lyapunov function. First, because it is difficult for a single LPV subsystem to satisfy a scene where the system parameters vary at a large scale, the lateral dynamics of the FAGV were modeled as a polyhedron LPV model. In this way, the parameter subregions were divided and used to derive a switching LPV control model. In addition, a gain-scheduling switching control

law was designed to increase control flexibility while avoiding the Zeno phenomenon. The proposed time-varying multi-parameter correlation Lyapunov function ensures closed-loop stability during the entire switching process. Finally, the feasibility and effectiveness of the proposed control method were verified on an industrial FAGV.

This paper focuses on the self-triggered switching control of FAGVs with time-varying parameters. However, the limited bandwidth and fluctuations of the network used for information transmission may introduce time-varying delays that can negatively affect system stability. Therefore, future research will investigate stabilized switching control methods for FAGVs under these circumstances.

Acknowledgments

This work is supported by the National Natural Science Foundation of China (Nos. 52105019, 52275488, and 52405563), the Key Research and Development Program of Hubei Province, China (No. 2022BAA064), the Science and Technology Innovation Talent Plan of Hubei Province (No. 2025DJA014), and the Key Research and Development Program of Wuhan, China (No. 2025061202030429).

Author contributions

Yuanlong XIE: writing—original draft, writing—review & editing, conceptualization, methodology, and funding acquisition. Shuting WANG: resources, investigation, funding acquisition, supervision, and project administration. Liquan JIANG: writing—original draft, software, conceptualization, and funding acquisition. Hu LI: software, formal analysis, and investigation. Hao WU: data curation, validation, and visualization. Sheng-quan XIE: supervision.

Conflict of interest

Yuanlong XIE, Shuting WANG, Liquan JIANG, Hu LI, Hao WU, and Sheng-quan XIE declare that they have no conflict of interest.

References

- Abbas HS, 2024. Linear parameter-varying model predictive control for nonlinear systems using general polytopic tubes. *Automatica*, 160:111432. <https://doi.org/10.1016/j.automatica.2023.111432>
- Arega TB, Tesfa YM, Abdissa CM, 2025. Three-wheeled mobile robot trajectory tracking control using nonlinear pid controller based neural network combined with backstepping controller. *IEEE Access*, 13:100167-100182. <https://doi.org/10.1109/ACCESS.2025.3577269>
- Cui D, Ahn CK, Xiang ZR, 2023. Fault-tolerant fuzzy observer-based fixed-time tracking control for nonlinear switched systems. *IEEE Transactions on Fuzzy Systems*, 31(12):4410-4420. <https://doi.org/10.1109/TFUZZ.2023.3284917>
- Dehghani M, 2024. Decentralized stabilization of large-scale linear parameter varying systems. *ISA Transactions*, 148:336-348. <https://doi.org/10.1016/j.isatra.2024.03.007>
- Dersch B, Negash L, Abdissa CM, 2023. Robust PSO tuned FOSMC for altitude stabilization and trajectory tracking of agricultural monitoring UAV. *TechRxiv*:24250348. <https://doi.org/10.36227/techrxiv.24250348.v1>
- Ding SH, Liu L, Zheng WX, 2017. Sliding mode direct yaw-moment control design for in-wheel electric vehicles. *IEEE Transactions on Industrial Electronics*, 64(8):6752-6762. <https://doi.org/10.1109/TIE.2017.2682024>
- Dirara HG, Yareshe FT, Abdissa CM, 2025. Design and analysis of adaptive fuzzy super-twisting sliding mode controller for uncertain 2-DOF robotic manipulator. *IEEE Access*, 13:110241-110254. <https://doi.org/10.1109/ACCESS.2025.3581449>
- Esmaili B, Modares H, 2024. Risk-informed model-free safe control of linear parameter-varying systems. *IEEE/CAA Journal of Automatica Sinica*, 11(9):1918-1932. <https://doi.org/10.1109/JAS.2024.124479>
- Guo JH, Wang JY, Luo YG, et al., 2021. Takagi-Sugeno fuzzy-based robust H_∞ integrated lane-keeping and direct yaw moment controller of unmanned electric vehicles. *IEEE/ASME Transactions on Mechatronics*, 26(4):2151-2162. <https://doi.org/10.1109/TMECH.2020.3032998>
- Hu C, Wang RR, Yan FJ, 2016. Integral sliding mode-based composite nonlinear feedback control for path following of four-wheel independently actuated autonomous vehicles. *IEEE Transactions on Transportation Electrification*, 2(2):221-230. <https://doi.org/10.1109/TTE.2016.2537046>
- Ji Y, Zhang JZ, Lv C, et al., 2023. Fault-tolerant vehicle stability control based on active steering and direct yaw moment with finite-time constraint performance recovery. *IEEE Transactions on Vehicular Technology*, 72(12):15317-15329. <https://doi.org/10.1109/TVT.2023.3294972>
- Jiang LQ, Wang ST, Xie YL, et al., 2022. Decoupled fractional supertwisting stabilization of interconnected mobile robot under harsh terrain conditions. *IEEE Transactions on Industrial Electronics*, 69(8):8178-8189. <https://doi.org/10.1109/TIE.2021.3111557>
- Liang JH, Feng JW, Lu YB, et al., 2024. A direct yaw moment control framework through robust T-S fuzzy approach considering vehicle stability margin. *IEEE/ASME Transactions on Mechatronics*, 29(1):166-178. <https://doi.org/10.1109/TMECH.2023.3274689>
- Liu Q, Long LJ, 2022. Asymptotic stability with guaranteed safety for switched nonlinear systems: a multiple barrier functions method. *IEEE Transactions on Systems, Man, and Cybernetics: Systems*, 52(6):3581-3590. <https://doi.org/10.1109/TSMC.2021.3072425>
- Lu YB, Liang JH, Zhuang WC, et al., 2024. Four-wheel independent drive vehicle fault tolerant strategy using stochastic model predictive control with model parameter uncertainties. *IEEE Transactions on Vehicular Technology*, 73(3):3287-3299. <https://doi.org/10.1109/TVT.2023.3321779>
- Ma L, Mei KQ, Ding SH, 2023. Direct yaw-moment control design for in-wheel electric vehicle with composite terminal sliding mode. *Nonlinear Dynamics*, 111(18):17141-17156. <https://doi.org/10.1007/s11071-023-08760-9>
- Meng J, Wang ST, Jiang LQ, et al., 2023. Accurate and efficient self-localization of agv relying on trusted area information in dynamic industrial scene. *IEEE Transactions on Vehicular Technology*, 72(6):7148-7159. <https://doi.org/10.1109/TVT.2023.3241203>
- Menyechel Eneyew G, Ayalew Asfaw W, Merga Abdissa C, 2025. Optimized backstepping fuzzy sliding mode controller for trajectory tracking of mobile manipulator. *Engineering Reports*, 7(7):e70269. <https://doi.org/10.1002/eng2.70269>
- Metekia EW, Asfaw WA, Abdissa CM, et al., 2025. Control of a fixed wing unmanned aerial vehicle using a robust fractional order controller. *Scientific Reports*, 15(1):19954. <https://doi.org/10.1038/s41598-025-03552-0>
- Mohammed TK, Asfaw WA, Abdissa CM, et al., 2025. Constrained robust adaptive control design for fixed wing UAV under parameter uncertainties and external disturbances. *Engineering Research Express*, 7(2):025254. <https://doi.org/10.1088/2631-8695/add643>
- Nguyen MN, Van M, Mcilvanna S, et al., 2024. Model-free safety critical model predictive control for mobile robot in dynamic environments. *IEEE Transactions on Intelligent Vehicles*, 9(11):6830-6842. <https://doi.org/10.1109/TIV.2024.3389111>
- Peng HN, Wang WD, An Q, et al., 2020. Path tracking and direct yaw moment coordinated control based on robust MPC with the finite time horizon for autonomous independent-drive vehicles. *IEEE Transactions on Vehicular Technology*, 69(6):6053-6066. <https://doi.org/10.1109/TVT.2020.2981619>
- Qu S, He TY, Zhu GG, 2020. Engine EGR valve modeling

- and switched LPV control considering nonlinear dry friction. *IEEE/ASME Transactions on Mechatronics*, 25(3):1668-1678.
<https://doi.org/10.1109/TMECH.2020.2982315>
- Rotondo D, Ponsart JC, Theilliol D, 2022. Gain-scheduled observer-based consensus for linear parameter varying multi-agent systems. *Automatica*, 135:109979.
<https://doi.org/10.1016/j.automatica.2021.109979>
- Souza M, Wirth FR, Shorten RN, 2017. A note on recursive schur complements, block Hurwitz stability of Metzler matrices, and related results. *IEEE Transactions on Automatic Control*, 62(8):4167-4172.
<https://doi.org/10.1109/TAC.2017.2682032>
- Verhoek C, Berberich J, Haesaert S, et al., 2024. Data-driven dissipativity analysis of linear parameter-varying systems. *IEEE Transactions on Automatic Control*, 69(12):8603-8616.
<https://doi.org/10.1109/TAC.2024.3417855>
- Vošahlík D, Haniš T, 2023. Traction control allocation employing vehicle motion feedback controller for four-wheel-independent-drive vehicle. *IEEE Transactions on Intelligent Transportation Systems*, 24(12):14570-14579.
<https://doi.org/10.1109/TITS.2023.3295436>
- Wang X, Zhao J, 2017. Autonomous switched control of load shifting robot manipulators. *IEEE Transactions on Industrial Electronics*, 64(9):7161-7170.
<https://doi.org/10.1109/TIE.2017.2688958>
- Xie YL, Zhang XL, Zheng SQ, et al., 2022. Asynchronous H_∞ continuous stabilization of mode-dependent switched mobile robot. *IEEE Transactions on Systems, Man, and Cybernetics: Systems*, 52(11):6906-6920.
<https://doi.org/10.1109/TSMC.2021.3119054>
- Yang ZY, Xu XH, Wang X, et al., 2024. Optimal configuration for mobile robotic grinding of large complex components based on redundant parameters. *IEEE Transactions on Industrial Electronics*, 71(8):9287-9296.
<https://doi.org/10.1109/TIE.2023.3314871>
- Yareshe FT, Madebo NW, Abdissa CM, et al., 2025. Trajectory tracking of fixed-wing UAV using ANFIS-based sliding mode controller. *IEEE Access*, 13:61986-62003.
<https://doi.org/10.1109/ACCESS.2025.3557472>
- Zeng TY, Mohammad A, Madrigal AG, et al., 2024. A robust human-robot collaborative control approach based on model predictive control. *IEEE Transactions on Industrial Electronics*, 71(7):7360-7369.
<https://doi.org/10.1109/TIE.2023.3299046>
- Zhang B, Zhao WZ, Wang CY, et al., 2023. Layered time-delay robust control strategy for yaw stability of SbW vehicles. *IEEE Transactions on Intelligent Vehicles*, 8(7):3913-3924.
<https://doi.org/10.1109/TIV.2023.3273540>
- Zhang JD, Zhang LP, Liu SS, et al., 2024. Cooperative control of active suspension and four-wheel steering for intelligent electric vehicles with corner module structure on severe roads. *IEEE Transactions on Intelligent Vehicles*, 9(12):7876-7884.
<https://doi.org/10.1109/TIV.2024.3403904>
- Zhang S, Puig V, Ifqir S, 2024. Robust LPV fault diagnosis using the set-based approach for autonomous ground vehicles. *IEEE Transactions on Intelligent Transportation Systems*, 25(8):9078-9090.
<https://doi.org/10.1109/TITS.2024.3394518>
- Zhao JP, Yang GH, 2024. Fuzzy adaptive finite-time resilient control against unknown false data injection attacks for MIMO nonlinear switched systems with unknown dead zone. *IEEE Transactions on Cybernetics*, 54(1):586-598.
<https://doi.org/10.1109/TCYB.2023.3258490>
- Zhao XQ, Liu Z, Jiang BP, et al., 2023. Switched controller design for robotic manipulator via neural network-based sliding mode approach. *IEEE Transactions on Circuits and Systems II: Express Briefs*, 70(2):561-565.
<https://doi.org/10.1109/TCSII.2022.3169475>

Electronic supplementary materials

Sections S1–S3; Eqs. (S1)–(S26)